Ann. Geophys., 26, 813–822, 2008
www.ann-geophys.net/26/813/2008/

Annales Geophysicae

Universal and local time components in Schumann resonance intensity

A. P. Nickolaenko[1] **and M. Hayakawa**[2]

[1]Usikov Institute for Radio-Physics and Electronics, National Academy of Sciences of the Ukraine, Kharkov 61085, Ukraine
[2]The University of Electro-Communications, Department of Electronic Engineering, Chofu-shi, Tokyo, 182-8585, Japan

Received: 4 April 2007 – Revised: 28 February 2008 – Accepted: 13 March 2008 – Published: 13 May 2008

Abstract. We extend the technique suggested by Sentman and Fraser (1991) and discussed by Pechony and Price (2006), the technique for separating the local and universal time variations in the Schumann resonance intensity. Initially, we simulate the resonance oscillations in a uniform Earth-ionosphere cavity with the distribution of lightning strokes based on the OTD satellite data. Different field components were used in the Dayside source model for the Moshiri (Japan, geographic coordinates: 44.365° N, 142.24° E) and Lehta (Karelia, Russia, 64.427° N, 33.974° E) observatories. We use the extended Fourier series for obtaining the modulating functions. Simulations show that the algorithm evaluates the impact of the source proximity in the resonance intensity. Our major goal was in estimating the universal alteration factors, which reflect changes in the global thunderstorm activity. It was achieved by compensating the local factors present in the initial data. The technique is introduced with the model Schumann resonance data and afterwards we use the long-term experimental records at the above sites for obtaining the diurnal/monthly variations of the global thunderstorms.

Keywords. Meteorology and atmospheric dynamics (Atmospheric electricity; Lightning) – Radio science (Remote sensing)

1 Introduction

Global electromagnetic (Schumann) resonance occurs in the thin dielectric shell separating the conducting ground and the ionosphere plasma. It is observed as peaks in the intensity of natural radio noise at frequencies around 8, 14, 20 Hz, etc. The energy is supplied by electromagnetic radiation from the lightning strokes distributed worldwide. Owing to low losses a radio wave can circle the globe several times, and the intensity recorded reflects the level of global thunderstorm activity. Observations at a field site are characterized by two factors: one depends on the universal time (the global thunderstorm intensity) and the other is the function of the local time (local ionosphere height, position of thunderstorms relative the observatory, etc.). The first depends on the Universal Time (t_U), while the second is a function of the Local Time (t_L).

When monitoring the global thunderstorm activity by using Schumann resonance (SR), one has to reduce the role of the local factors and preserve the universal modulations. For this purpose, the cumulative resonance intensity was suggested and used by Polk (1969), which is the resonance field intensity integrated over a few SR modes. The advantage of cumulative intensity is conditioned by smoothing the distance dependence pertinent to different resonant modes. Model computations showed that an effect of diurnal motion of global thunderstorms decreases from ∼10 dB variation in the individual modes toward ∼3 dB in the cumulative intensity (Nickolaenko, 1997). Thus, the role of source proximity is reduced by the cumulative intensity, but it is not removed completely. In the present paper, we modify a technique that separates the local and universal factors and estimate the level of global thunderstorms by using the cumulative SR intensity recoded at a pair of longitudinally separated observatories.

A first comparison of SR intensities recorded at two widely separated observatories was made by Polk and Fitchen (1962), in which measurements were made at Brannenburg (Germany) and Kingston (R.I., USA). Their experiment indicated that diurnal variations at two points look more similar when plotted against the local time rather than in the universal time.

The formal procedure for extracting the local and universal factors from a record at two observatories was suggested by Sentman and Fraser (1991). They applied it to the

Correspondence to: M. Hayakawa
(hayakawa@whistler.ee.uec.ac.jp)

Published by Copernicus Publications on behalf of the European Geosciences Union.

experimental cumulative intensity and singled out the periodic local factor. The sites were positioned at California and Australia. The local changes derived were attributed to alterations in the local ionosphere height above each site.

The further step was made by Pechony and Price (2006), who computed the intensity of the global resonance in the model of a uniform Earth-ionosphere cavity and demonstrated that local modulations still remain in the model data. They used the time varying thunderstorm distributions in model that follow from the records of Optical Transient Detector (OTD) satellite. Thus the above work showed that the local time variations arise from a diurnal motion of thunderstorm activity around the globe, i.e. from the source proximity. Magnitude of model variations was close to that observed experimentally by Sentman and Fraser (1991).

The goal of the present publication is two-fold. First, we adopt a similar technique to the case of a slightly different source distribution in comparison with Pechony and Price (2006). Such a numerical experiment allows us to test the robustness of our processing. Second, we extend the number of terms in the Fourier expansion from 1 to 5 and therefore acquire more sophisticated temporal variations. The processing technique is also developed aiming on the direct extraction of universal or local time factors.

Initially, we describe the procedure and process a model signal to demonstrate applicability of the technique. The model intensity variations were computed in the uniform Earth-ionosphere cavity with the thunderstorm distribution based on the global OTD maps of lightning flashes (Hayakawa et al., 2005; Nickolaenko et al., 2006; Pechony et al., 2006). We compare the "postulated" source intensity with the universal factor "deduced" from the SR and thus evaluate the accuracy. The algorithm is finally applied to the long-term experimental records of SR at the same two points and the estimates are found for diurnal/monthly variations of the global thunderstorm activity for the period one year long.

2 Formal treatment

Similarly to Sentman and Fraser (1991), we accept that

(i) Intensity of SR $P\,(t_U, \lambda)$ recorded in the universal time t_U and at the east longitude λ is a product of the universal function $U\,(t_U)$ and the local modulating function $L\,(t_L)$:

$$P\,(t_U) = U\,(t_U) \cdot L\,(t_L) \tag{1}$$

Additionally, we present the same data against the local time t_L, which is used later for the direct extracting of the universal component instead of the local time variation:

$$Q\,(t_L) = U\,(t_U) \cdot L\,(t_L) \tag{2}$$

Here $P\,(t_U)$ denotes the SR intensity recorded in the universal time t_U, $Q\,(t_L)$ is the same intensity as the function of the local time of the observatory t_L that occupies the east longitude λ. $U\,(t_U)$ and $L\,(t_L)$ are the universal and local factors to be found. Equations (1) and (2) are used for an arbitrary observatory.

(ii) The following relation is valid (Sentman and Fraser, 1991):

$$t_L = t_U + \lambda, \tag{3}$$

with all quantities measured in radians and ranging from 0 to 2π.

(iii) Functions P and Q at an observatory are the same functions of time. The only distinction is in the shift along the abscissa in correspondence with Eq. (3). Of course, deviations might occur in the data calibration P_1, Q_1 and P_2 and Q_2 at different observatories. These might cause different amplitude scaling (similar distinctions might arise from the different latitudes of the sites).

(iv) Since functions $U\,(t_U)$ and $L\,(t_L)$ have a period of 2π, we expand them into the following Fourier series:

$$L_1\,(t_U) = 1 + \sum_{k=1}^{\infty} A_k \exp\left[ik\,(t_U + \lambda_1)\right]$$

$$L_2\,(t_U) = 1 + \sum_{k=1}^{\infty} A_k \exp\left[ik\,(t_U + \lambda_2)\right] \tag{4}$$

Similarly, we develop relations for the universal modulating functions. The procedure is also the Fourier expansion and only initial SR intensities must be presented versus the local time of observatories instead of the UT. Formally, we obtain the following series for the normalized universal modulating factors:

$$u_1\,(t_L) = 1 + \sum_{k=1}^{\infty} B_k \exp\left[ik\,(t_L - \lambda_1)\right]$$

$$u_2\,(t_L) = 1 + \sum_{k=1}^{\infty} B_k \exp\left[ik\,(t_L - \lambda_2)\right] \tag{5}$$

Here, L_1 and L_2 is the local modulations at each site. The functions are found by using Eq. (1). The normalized universal modulating factors at the sites are denoted as u_1 and u_2, they depend on the local time of observatories, and will be found by using $Q_1(t_L)$ and $Q_2(t_L)$ records.

Soundness of "similarity" assumption (iii) becomes evident when one compares plots (a) and (c) in Fig. 1. Here we depict the model diurnal variations of cumulative SR intensity in the vertical electric field component. The field intensity is shown along the ordinate (the lower frame shows the flash number, see below). The time is plotted on the abscissa. Each frame in Fig. 1 combines diurnal and seasonal variations. For the purpose, the abscissa is divided into 12 intervals each corresponding to a month of a year. The names of months are printed above the strips. The 24 h diurnal patterns are depicted in every "monthly" interval. Particular diurnal variations were computed for the 15th day of each month. Thus, one observes in Fig. 1 both the diurnal variations and monthly modifications.

The upper frame (a) in Fig. 1 depicts the $Q\ (t_L)$ – functions, the third frame (c) presents the $P\ (t_U)$ – variations. Coordinates of two observatories were used. One is Lehta (geographic coordinates: 64.427° N and 33.974° E), whose data are shown by blue curves. The second is Moshiri (44.365° N and 142.24°), with the relevant graphs in the magenta lines. As one may observe, the plots vary similarly against the UT, i.e. in Fig. 1c. Mutual departures of two curves in the UT are demonstrated by Fig. 1b in form of the ratio $P_1(t_U)/P_2(t_U)$. We return to the data of Fig. 1 later. Here, we must note a higher similarity of the patterns in the UT, which validates the assumption (iii).

Expansion (4) corresponds to the formula used by Sentman and Fraser (1991). The distinction is that they have used a single harmonic only. We use the five terms expansions $k\in[1; 5]$. Similarly to Sentman and Fraser (1991), we use the UT records $P_1(t_U)$ and $P_2(t_U)$ for deriving the local time factors (Eq. 4). The expansion coefficients are found from the following equation:

$$A_k = \frac{1}{2\pi\left[\exp(ik\lambda_1) - \exp(ik\lambda_2)\right]} \int_0^{2\pi} \ln\left[\frac{P_1(t_U)}{P_2(t_U)}\right] \exp(-ikt_U)\, dt_U \tag{6}$$

The local factors $L_1(t_U)$ and $L_2(t_U)$ are reconstructed with the coefficients A_k substituted into Eq. (4).

Our goal is obtaining universal variations $U_1(t_U)$ and $U_2(t_U)$ representing the current intensity of the global thunderstorms. To find the universal factors directly, we apply the SR records (Eq. 2) performed in the local times $Q_1(t_L)$ and $Q_2(t_L)$. The expansion coefficients for the "normalized" universal factors are:

$$B_k = \frac{1}{2\pi\left[\exp(-ik\lambda_1) - \exp(-ik\lambda_2)\right]} \int_0^{2\pi} \ln\left[\frac{Q_1(t_L)}{Q_2(t_L)}\right] \exp(-ikt_L)\, dt_L \tag{7}$$

After finding quantities B_k, we construct functions $u_1(t_L)$ and $u_2(t_L)$ by using Eq. (5), and afterwards we compute the genuine functions $U_1(t_L)$, $U_2(t_L)$:

$$U_m(t_L) = u_m(t_L) \cdot \overline{Q}_m(t_L) \quad m = 1,\ 2 \tag{8}$$

with the average intensity at a site:

$$\overline{Q}_m(t_L) = \frac{1}{2\pi} \int_0^{2\pi} Q_m(t_L)\, dt_L. \tag{9}$$

Finally, the local times t_L of observatories are translated into the universal time, and we obtain the functions $U_1(t_U)$ and $U_2(t_U)$. The last procedure provides two "independent" estimates for the global thunderstorm activity. Their consistency reflects the robustness of the procedure.

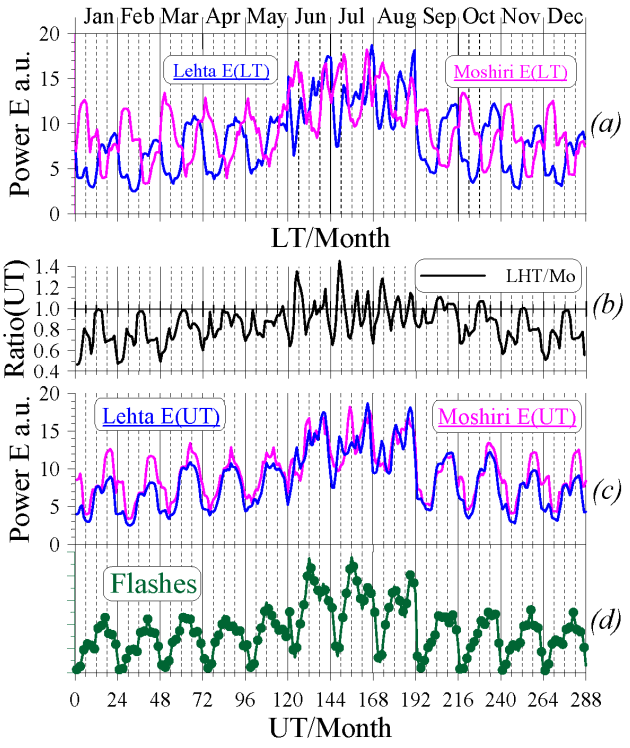

Fig. 1. A set of twelve model diurnal patterns, each corresponding to a month. Frame **(a)** depicts the $Q\ (t_L)$ data and frame **(c)** is the $P\ (t_U)$ variations. Intensities are measured in arbitrary units. Data for Lehta are shown by blue line and for Moshiri – by magenta line. Plot **(b)** depicts the intensity ratio $P_{\rm LEHTA}/P_{\rm MOSHIRI}$, and the lower green dotted curve presents the source intensity.

By comparing Eqs. (6) and (7), we find only minor distinctions. The sign has changed of the "longitudinal" argument in the denominator; the integration is performed over t_U in Eq. (6) and over t_L in Eq. (7). Since this is the "umbral" argument, the result does not depend on the type of particular variable. Hence, expansions of the local and the normalized universal functions are obtained by essentially the same procedure. The key distinction is that initial data are related to the LT when we obtain the universal factor, and to the UT when we obtain the local modulation factor.

We use below the SR records 24 h long, and an extension to a wider interval is rather straightforward. The Fourier coefficients might be computed directly or by using the standard FFT procedure.

To conclude the formal description, we mention the simplest possible signal processing: the geometrical averaging. Let us assume that two observatories have the longitudinal separation of 180° or $(\lambda_1 - \lambda_2) = \pm\pi$. The basic terms in the local modulating functions $L_1(t_L)$ and $L_2(t_L)$ having the 24 h period will be equal in amplitude and have the opposite sign. As a result, the sum of intensity logarithms retains only the

universal terms:

$$S = \ln[P(t_U, \lambda)] + \ln[P(t_U, \lambda + \pi)] \approx U(t_U)[1 + ReA_1(t_U)] + U(t_U)[1 - ReA_1(t_U)] = 2U(t_U) \quad (10)$$

Equation (10) indicates that geometrical averaging of intensities

$$GA = \sqrt{P(t_U, \lambda_1) \cdot P(t_U, \lambda_2)} \quad (11)$$

represents the "rectified" universal variations. Physical explanation of this effect is simple: when storms come closer to one observatory, they simultaneously retreat from the other, so that the product of individual SR intensities tends to be independent of the source distance. When $(\lambda_1 - \lambda_2) = \pm\pi$, we exactly have $GA = U(t_U)$. When observatories are separated in longitude by a smaller value (or their latitudes are different), the compensation is incomplete of the local modulations.

The idea of geometric averaging is easily extended to the case of many sites. For instance, when we have three observatories (separated by $2\pi/3$ in longitude), the global thunderstorm intensity is evaluated by $U(t_U) = \sqrt[3]{P_1 \cdot P_2 \cdot P_3}$, etc. Simple geometrical averaging of the UT data provides an estimate for the intensity of the global thunderstorms. Vice versa, the procedure applied to intensities recorded in the local time provides an estimate for the local modulating function. We show with the model data that geometrical averaging is as efficient as a more complicated Fourier expansion algorithm.

3 Modeling of the SR data

After formulating the main points of data processing, we turn to computing the SR spectra and obtaining variations of cumulative intensity at two points of longitudes λ_1 and λ_2. In particular, we use observatories separated both in longitudes and latitudes: Lehta (Karelia) and Moshiri (Hokkaido). We use the uniform model of Earth – ionosphere cavity. Frequency dependence of the propagation constant is approximated by the following linear function (Nickolaenko and Hayakawa, 2002):

$$\nu(f) = \frac{f - 2}{6} - i\frac{f}{70} \quad (12)$$

Let us test the above modifications of the Sentman and Fraser (1991) approach. In addition we compare our data with conclusions by Pechony and Price (2006) based on a different source model.

One might use, say, the single point source model (Yatsevich et al., 2006) for the purpose, or the model of three global thunderstorm centers (Nickolaenko et al., 1998) and synthesize the necessary "experimental" data set. Clearly, the model data should be realistic, therefore, we use the following approach. The global thunderstorm distribution was observed from space by the Optical Transient Detector (OTD) (Christian et al., 2003), and we use the low resolution full climatology dataset with the step of 2.5 by 2.5 degrees. To introduce the daily motion of thunderstorms, we apply the Dayside (DS) model (Nickolaenko et al., 2006; Pechony et al., 2006). This model is the mask covering the dayside of the globe for the specific date and the time (UT). The mask is applied to the OTD map relevant to a particular month, and the lightning flashes are "active" within the dayside, while those at the night side do not occur. The mask circles the globe during the day, thus the daily motion of thunderstorm activity appears in the averaged optical observations from space. To improve correspondence to the reality, we "rotate" the DS mask toward the evening terminator so that its center (the potential peak of activity) is placed at 17:00 LT.

Strokes within individual cells of the OTD map are independent and form a Poisson succession of electromagnetic pulses, therefore, their intensities are summed. The contribution from a particular cell is directly proportional to the number of flashes here. Such a model allows for computing the intensity of any field component or any second-order mixed statistical moments of the fields (Nickolaenko et al., 2006; Pechony et al., 2006). We computed the power spectra of E_Z field component at a site for the given hour UT and for the 15th day of each month. Afterwards, we integrated the field intensities in the frequency band from 4 to 26 Hz and obtained the functions $P_1(t_U)$, $P_2(t_U)$ and $Q_1(t_L)$, $Q_2(t_L)$ plotted in Fig. 1.

Every frame in Fig. 1 combines 12 diurnal patterns shown against the local (Fig. 1a) and universal time (Fig. 1c). The 24 h diurnal alterations follow each other in correspondence with the month starting from January.

Model diurnal patterns at two distant observatories have much in common. Field intensity noticeably increases during the summer. As we already noted, alterations become especially similar when plotted against the universal time (see Fig. 1c), which confirms the general idea that the cumulative SR intensity closely represents the global thunderstorm activity. The lower plot (Fig. 1d) is a reference, and it depicts the cumulative number of lightning flashes recorded by the OTD satellite. The model source intensity is proportional to this quantity. In an ideal case, when the spatial modal structure of resonance oscillations is completely compensated, the SR records must coincide with the reference curve. Our computations indicate that reciprocity undoubtedly exists, but curves do not coincide completely.

4 Extracting the local factors

As the first step, we process the model data similarly to Sentman and Fraser (1991) and Pechony and Price (2006). The

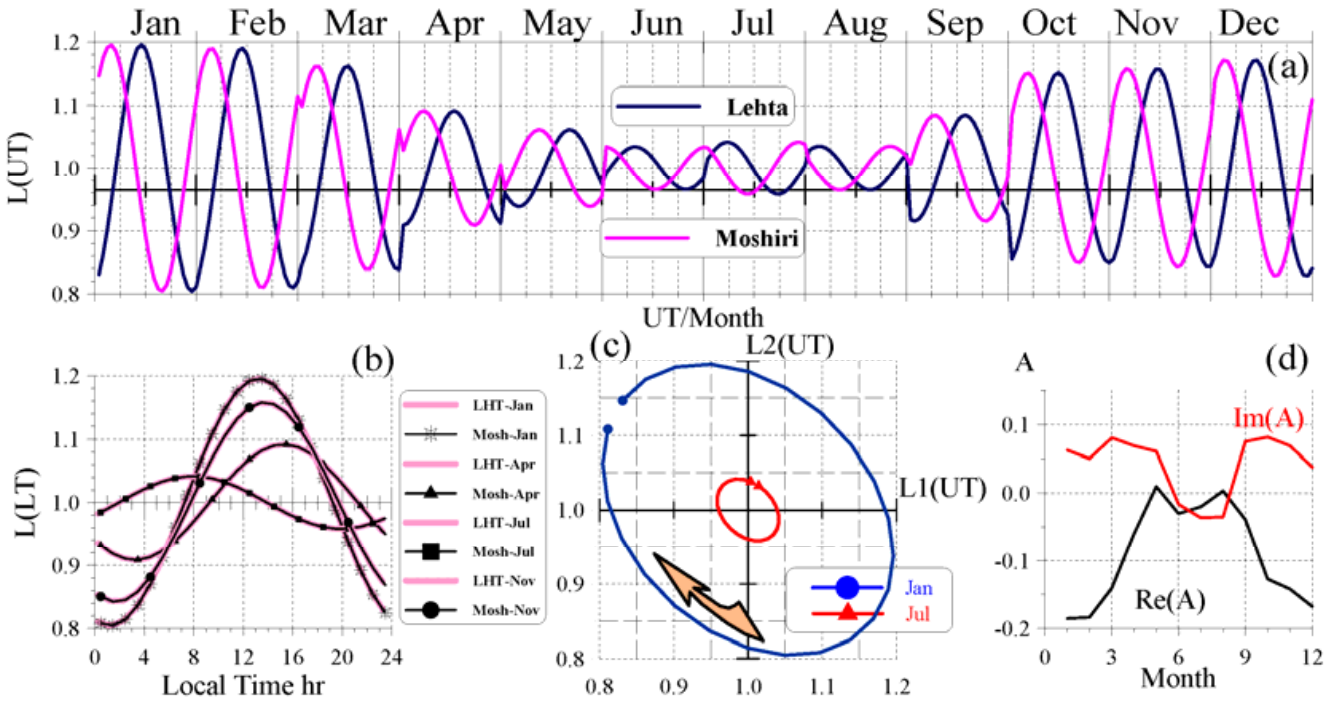

Fig. 2. Local modulation functions for model Schumann resonance records at Lehta and Moshiri extracted by the Sentman and Fraser (1991) algorithm. A single term in the Fourier series.

initial data are the functions of the universal time, and we exploit only the A_1 Fourier coefficient.

Figure 2a surveys monthly/diurnal alterations of the modulating functions L_1 (Lehta) and L_2 (Moshiri) versus UT. Again, twelve diurnal patterns are shown, each corresponding to different month. We observe that local modulations increase in winter and decrease in summer, and the position of peak depends on the season. Figure 2b compares the same variations plotted in the local time. The wide pink lines here depict the Lehta data, while results for Moshiri are plotted by narrow black marked lines. Characteristic months were chosen: January, April, July, and November. We must recall here that Sentman and Fraser (1991) have noted an outstanding similarity of these curves and attributed them to variations of the local ionosphere height. Such an interpretation looks reasonable if we accept that cumulative SR intensity is completely independent of the source – observer geometry. Unfortunately, this is not so because the ionosphere height is an invariant in our model of the uniform cavity and only source motion might cause variations in our data. Thus our computations support the conclusion by Pechony and Price (2006) based on different cavity and the source model. Physically, Fig. 2 shows that cumulative resonance intensity does not completely remove the modal structure, and the effect of source proximity is still present in the data.

Figure 2c shows the impact of seasonal redistribution of global thunderstorms on the peak positioning in the L-functions. We use January and July data here depicted as Lissajous plots (time UT$\in$[1; 24] is the parameter). The arrow shows the clockwise temporal motion of the representing point; the starting and the final points are marked. One may see that only two parameters of ellipses vary with season: the size and position of initial/ending points. Ellipticity and orientation of the curve remain stable regardless the seasonal drift of thunderstorms. The ellipticity depends on the longitude separation of the sites, and the Lissajous plots are the wide ellipses for λ_1–λ_2=110°. For the 90° separation the plot would become a circle, and it is the straight line for 180 degrees. Such a behavior of our model data agrees with the experimental results published by Polk and Fitchen (1962). Figure 2d explains why the initial phase of sinusoidal pattern varies with the month: alterations are caused by changes in the imaginary and real parts of the complex A_1 amplitude. The black line depicts Re$\{A_1\}$, and the red line shows Im$\{A_1\}$.

We conclude that our model data support the conclusion made by Pechony and Price (2006): the local time variations remain in the cumulative SR intensity, and these alterations are connected with the diurnal/seasonal motion of thunderstorms around the globe.

After repeating the processing suggested by Sentman and Fraser (1991), we extend the number of Fourier coefficients in an attempt to obtain the detailed variations. We use five harmonics in Eq. (6) and substitute these into the series (4). Relevant local modulating functions L_1 and L_2 are shown in Fig. 3. The upper frame (Fig. 3a) depicts the monthly/diurnal

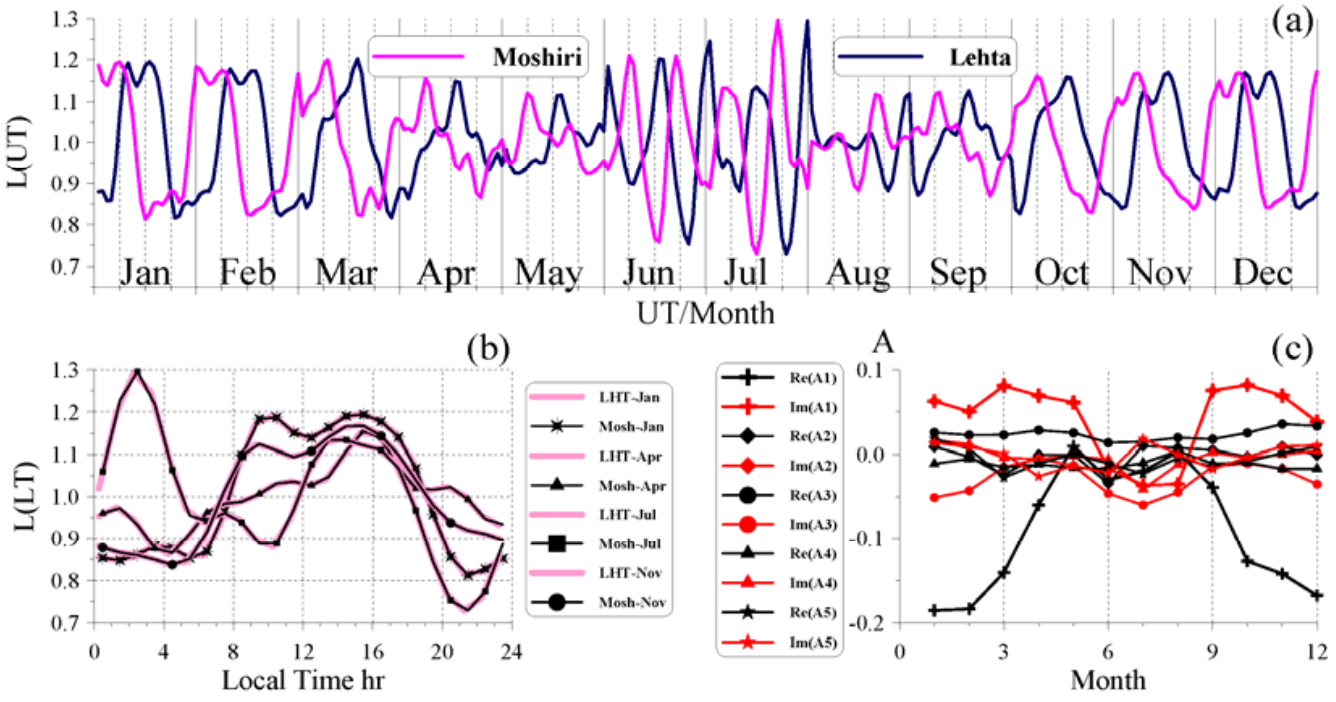

Fig. 3. Local modulation functions for Lehta and Moshiri obtained with a series of five terms in the Fourier series.

modulations against UT. One can observe that additional terms substantially modify the patterns. Now, the smallest modulation occurs in the intermediate seasons, which is in accord with observations of the first SR frequency: the thunderstorms "spread" over the globe during the intermediate seasons (Nickolaenko and Rabinowicz, 1995; Nickolaenko et al., 1998).

Figure 3b shows the modulation factors L_1 and L_2 against the local time. We plot the Lehta data by wide magenta lines, and those for Moshiri by the narrow black marked lines. The same four characteristic months were used for the seasons. One may observe that plots became complicated, however, their similarity was preserved. It is interesting to note that Fig. 3b indicates the smallest source – observer distance around 16:00 LT, which agrees with the general description of thunderstorm development. The morning peak around 10:00 h probably reflects the thunderstorm activity in the South-East Asia. The nighttime summer peak should be attributed to thunderstorm activity at the West coast of the North America. Since we perform a "controlled" numerical experiment, we can readily check the above interpretations with the OTD maps and with the relevant variations in the flash number (Nickolaenko et al., 2006; Pechony et al., 2006). Figure 3c illustrates the behavior of the complex A_n coefficients for five Fourier terms $n \in [1; 5]$.

We can derive the universal functions U_1 and U_2 now by dividing initial intensities P_1 and P_2 by modulating functions L_1 and L_2. This is an obvious way for obtaining the universal modulations as a proxy of the global thunderstorm activity. The U_1 and U_2 functions obtained will be regarded as "recovered", which are depicted in Fig. 5a. Functions U alter similarly in general, and deviations appear in summer. However, correspondence of the U_1 and U_2 patterns in Fig. 5a is less pronounced than that of the local modulating functions L. Plots (c) in Fig. 5 show that geometric averages are also close to each other and to the recovered universal modulations. Data are also similar to the "input" source intensity shown by the lowest line in Fig. 5d. We must note that simple geometrical averaging procedure provides results as good as more complicated procedures of evaluating the L-functions first and deriving the U-function afterwards.

5 Extracting the model universal factors

We described an alternative variant of the data processing, which is based on Eqs. (5) and (7). It allows us to directly reconstruct variations of the universal factors $u_1(t_L)$ and $u_2(t_L)$. The results are presented in Fig. 4a in the manner similar to that of Fig. 3a. Figure 4a surveys the diurnal/monthly alterations of the "normalized thunderstorm activity" against the local times of Lehta (dark blue line) and Moshiri (magenta curve). As we see, the estimated source activity varies substantially up to ten times, and the peak-to-peak alterations decrease almost to two-fold level during the summer season.

Similarly to the local modulating functions, the normalized universal variations are close to each other when

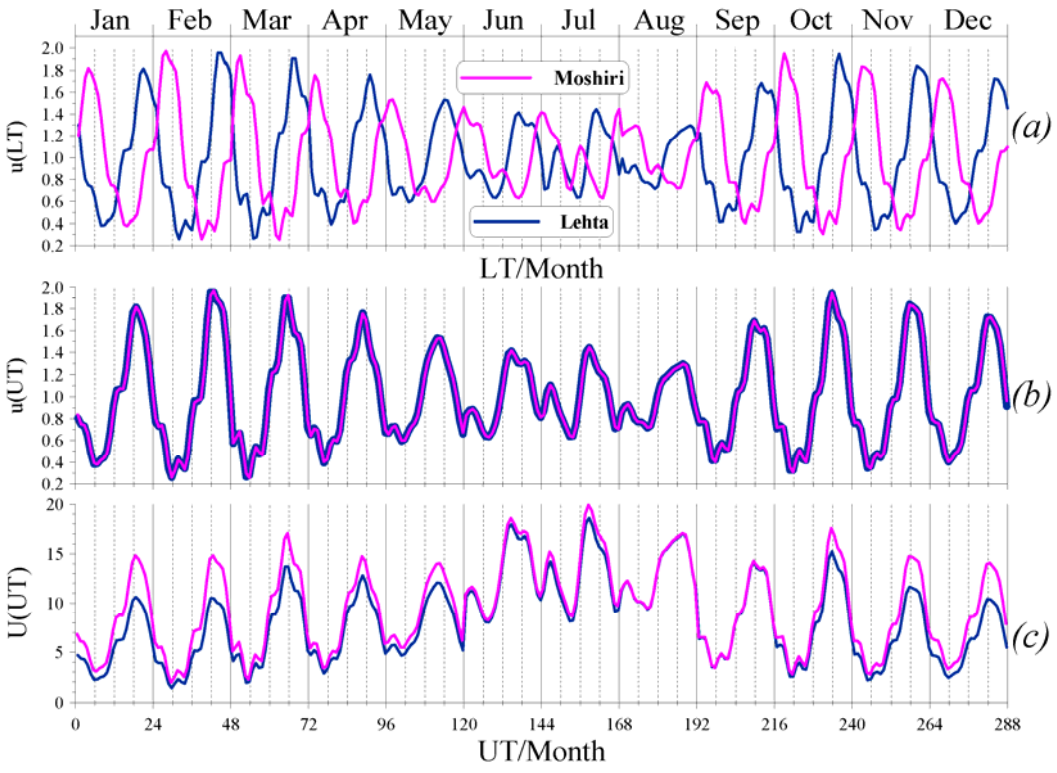

Fig. 4. Universal modulation functions: the normalized – $u(UT)$ and the "absolute" – $U(UT)$ obtained from the Lehta and Moshiri model data with a series of five terms.

translated from the LT to UT with the help of Eq. (3). Figure 4b compares the daily patterns $u_1(t_U)$ and $u_2(t_U)$ for twelve months of a year. Wide blue line presents the Lehta data, and data for Moshiri are depicted by magenta line. Plots in Fig. 4b practically coincide. After multiplying the normalized patterns by the daily average intensities at relevant sites (9), we obtain the "absolute" curves $U_1(t_U)$ and $U_2(t_U)$ presented in Fig. 4c. The "scaling factor" separates individual patterns. The coincidence is retained for some months. Deviations are conditioned by an inequality of the median distance from the sources to the observatories: we use the sites separated not only by the longitude, but also along the latitude. In experimental studies, similar deviations might also arise from departures in the data calibration.

6 Comparison of universal patterns recovered

We compare in Fig. 5 all kinds of variations obtained for the universal time factors U. The upper plots show the "recovered" data when the local modulations were found first, and the functions $U_1(UT)$ and $U_2(UT)$ were derived by compensating the local modulations $L_1(UT)$ and $L_2(UT)$ in the records $P_1(t_U)$ and $P_2(t_U)$. The dark blue curve corresponds to the Lehta data and the magenta line depicts those of Moshiri. The green line is the reference curve: the postulated

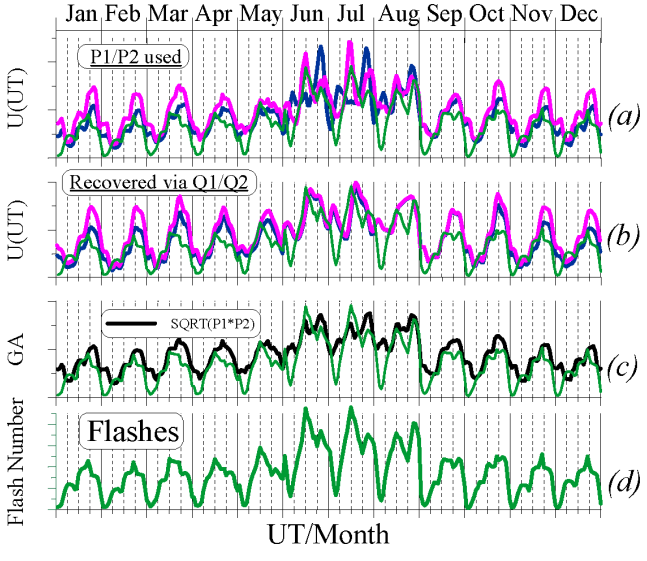

Fig. 5. Survey of universal modulations. Curves **(a)** depict the results after compensating the local factors L. Curves **(b)** show the results of direct evaluation of U(UT) by using the Q_1/Q_2 ratio. Curve **(c)** is the geometric average $GA(t_U)$, and curve **(d)** depicts the model source intensity.

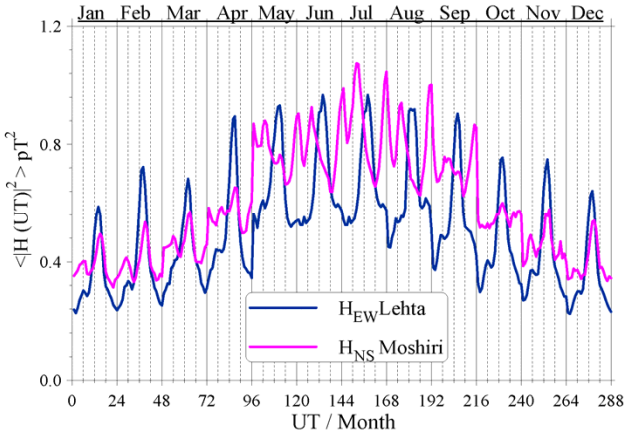

Fig. 6. Experimental data of H_{EW} component at Lehta and the H_{NS} field at Moshiri.

source intensity or the cumulative flash number used in computations.

Figure 5b depicts the results of another variant of data processing when the UT modulation is directly reconstructed from the resonance intensities $Q_1(t_L)$ and $Q_2(t_L)$. Two curves in Fig. 5b are in a better agreement with the cumulative flash number than the previous pair of Fig. 5a. Improvement is especially pronounced in the summer months where the recovered curves of Fig. 5a seriously deviate from each other and from the flash number. The third panel, Figure 5c, shows the geometrical average $GA=\sqrt{P_1\,(t_U)\cdot P_2\,(t_U)}$ of the data. Again, the simple procedure proved to be efficient, and correspondence with the source intensity is as good as in plots (a) and (b). The lowest plot in Fig. 5 separately depicts the diurnal/seasonal alternations of the cumulative number of flashes.

As Fig. 5 demonstrates, patterns obtained by different schemes have much in common. All contain the typical feature of an afternoon maximum in the thunderstorm intensity, the increase during summer. General reciprocity is present in the postulated source intensity. It seems that plots (b) and (c) are slightly better than plot (a). However, every curve deviates from the flash number, and we cannot state that SR intensity enables an exact derivation of the global thunderstorm activity. One may speak about definite quantitative agreement with possible deviations of ±20%. Such an accuracy is not bad if we have in mind the global coverage and operational efficiency of the technique.

To conclude presentation of the model data, we must mention that SR computations were also made for two orthogonal horizontal magnetic field components. Similar processing was applied toward arbitrary combination of the fields "recorded" at Lehta and Moshiri, and the results were similar. This indicates robustness of the technique: the source intensity estimated is independent of the particular field component. This allows us to extend the above conclusion on the arbitrary combination of resonance spectra collected at distant observatories. Below, we apply the above procedures toward experimental data accumulated at Lehta and Moshiri.

7 Processing of the experimental data

Experimental data (see Fig. 6) were collected at the Lehta and Moshiri observatories. The dark blue line depicts the UT/monthly variations of resonance intensity in the H_{EW} component at Lehta and the pink line depicts the H_{NS} Moshiri record. Experimental data continuously cover the period from January 1999 to December 2001. We use the monthly averaged diurnal variations at a site. As Fig. 6 demonstrates, diurnal patterns of Lehta and Moshiri are similar, especially in winter. Deviations appear in the interval from May to September, probably caused by a contribution from the nearby lightning strokes: the fine structure of the Moshiri record might be conditioned by thunderstorms of the South-East Asia and the Northern Australia.

Figure 7 surveys the processing results of the experiment. Plots are depicted against the time/month argument as it was done before. Plot (a) in Fig. 7 presents the initial data $P_1(t_U)$ – Lehta (blue line) and $P_2(t_U)$ – Moshiri (pink line) as the functions of the universal time. According to Polk (1969) and Nickolaenko (1997), these plots are two independent estimates for the diurnal/seasonal alternations in the global thunderstorm activity.

Figure 7b shows the same data plotted against the local time of observatories: $Q_1(t_L)$ – Lehta (blue line) and $Q_2(t_L)$ – Moshiri (pink line). Figure 7c depicts the local modulating functions $L_1(t_L)$ and $L_2(t_L)$ derived with the five term Fourier expansion (4). These two functions coincide again. However, variations following from the SR measurements deviate from the model data of Fig. 4, thus indicating limitations of any, even sophisticated models. The local factors have patterns varying with season, and the highest modulation may exceed ±40% level even in the cumulative SR intensity.

The right plots in Fig. 7 present the universal modulation factors against the UT. Figure 7d depicts functions $U_1(t_U)$ – Lehta (blue line) and $U_2(t_U)$ – Moshiri (pink line). These were obtained by dividing the original records $P_1(t_U)$ and $P_2(t_U)$ by the local modulating functions $L_1(t_U)$ and $L_2(t_U)$. Figure 7e shows the universal factors obtained by the second variant of the processing: the direct extraction from the original records (5). Figure 7f shows the geometric average of experimental data in the UT.

By comparing the right plots of Fig. 7d–f, we note that variations of different universal factors have much in common. A closer inspection shows that diurnal changes in plot (d) seem to be too high, while the plot (f) does not show great enough variations in summer. The plot (e) occupies an intermediate position. All variations agree with the climatology data, however, individual patterns deviate in details. It

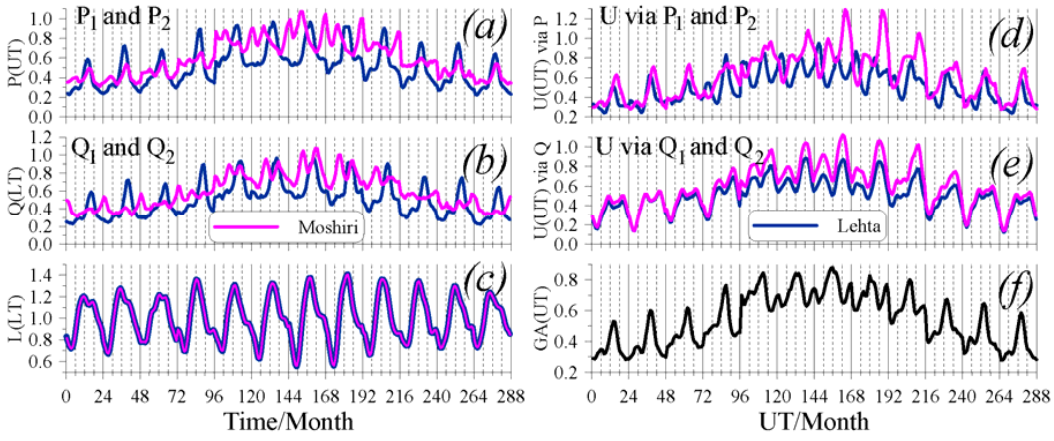

Fig. 7. Survey of experimental data from Lehta and Moshiri and of the local and universal modulations derived.

is important to mention a "podium" in the global lightning activity present in experiment. Owing to the podium, neither SR intensity nor the evaluated thunderstorm activity become very small (Yatsevich et al., 2006). This experimental result contradicts the expectations based on climatological perceptions. Indeed, the global thunderstorm activity is small over the oceans. The resonance signal should decrease by a factor of ten or so during the UT night when the Pacific thunderstorms (being practically absent) become the major field source. Instead, the observed intensity reduces, but only by a factor of 2 or 3 because the experimental curves are elevated over the abscissa, as if they are placed on a "podium". The level of such a podium increases in summer. Probably, the podium signal reflects the thunderstorm activity uniformly distributed over the globe (Yatsevich et al., 2006).

8 Conclusion

In the present paper, we extend the Sentman and Fraser (1991) technique suggested for separating the universal and the local factors in the SR intensity. We tested the technique on the model resonance data relevant to the uniform Earth-ionosphere cavity with the spatial distribution of lighting strokes based on the OTD satellite records. The Dayside Model was applied, and particular observatories were chosen at Moshiri (Japan) and Lehta (Russia).

Computations indicate that the integrated field intensity of resonance yet depends on the source distribution thus confirming conclusion by Pechony and Price (2006). The algorithm we use includes the higher-order Fourier terms, so that diurnal variations acquire complicated forms that alter with the season.

The major goal was extracting the universal modulating function, which reflects alterations in the global thunderstorm activity. Three variants were used for the purpose. The first one finds and compensates the local factors in the cumulative resonance intensity recorded in the universal time. The second variant directly extracts the universal factor from two records, each performed in the local time. The third one is a simple geometrical averaging of the input data presented in the UT. Computations show that all variants similarly improve the reciprocity to the model source intensity, but the coincidence is never achieved. Characteristic deviations are of $\pm 20\%$.

The same three variants of signal processing were applied toward the averaged long-term experimental data collected at Moshiri and Lehta observatories separated along the latitude and longitude by a great distance. Both local and universal modulating functions were deduced from the records. A comparison of the universal variations showed their qualitative similarity. Results of data processing show that none of these variants allows for exact deducing the instant level of the global thunderstorm activity from the SR. The accuracy of the estimates is about $\pm 20\%$. The geometrical averaging of the SR data acquired at distant sites is the simplest technique, which provides accuracy comparable with that of more complicated Fourier expansions.

Two particular observatories were used here to illustrate the idea. Additional studies are possible comparing different pairs of existing sites. Besides, an optimal positioning might be sought for the SR observatories that monitor the global thunderstorm activity. However, these interesting points deserve a separate treatment.

Summarizing the results of present study, we formulate the following recommendations for estimating the global thunderstorm activity from SR records:

1. Use at least five terms in Fourier expansions of the local and global factors. These might be helpful when obtaining traces of the global thunderstorm centers.

2. Take experimental data in the local time of the sites and directly extract the U-factors representing the global thunderstorms.

3. Include the geometric averaging of cumulative intensities recorded in the UT. Its closeness to the U-factors found with the Fourier expansions is a measure of accuracy of the "output" data.

Acknowledgements. We are grateful to Sekisui Chemical Foundation and NiCT (R&D promotion scheme funding international joint research) for their supports.

Topical Editor U.-P. Hoppe thanks one anonymous referee for her/his help in evaluating this paper.

References

Christian, H. J., Blakeslee, R. J., Boccippio, D. J., Boeck, W. L., Buechler, D. E., Driscoll, K. T., Goodman, S. J., Hall, J. M., Koshak, W. J., Mach, D. M., and Stewart, M. F.: Global frequency and distribution of lightning as observed from space by the Optical Transient Detector, J. Geophys. Res., 108(D1), 4005, doi:10.1029/2002JD002347, 2003.

Hayakawa, M., Sekiguchi, M., and Nickolaenko, A. P.: Diurnal variations of electric activity of global thunderstorms deduced from OTD data, J. Atmos. Electr., 25(2), 55–68, 2005.

Nickolaenko, A. P. and Rabinowicz, L. M.: Study of the annual changes of global lightning distribution and frequency variations of the first Schumann resonance mode, J. Atmos. Terr. Phys., 57, 1345–1348, 1995.

Nickolaenko, A. P.: Modern aspects of Schumann resonance studies, J. Atmos Sol.-Terr. Phy., 59, 805–816, 1997.

Nickolaenko, A. P., Sátori, G., Ziegler, V., Rabinowicz, L. M., and Kudintseva, I. G.: Parameters of global thunderstorm activity deduced from the long-term Schumann resonance records, J. Atmos. Sol.-Terr. Phy., 60, 387–399, 1998.

Nickolaenko, A. P. and Hayakawa, M.: Resonances in the Earth-ionosphere Cavity, Kluwer Academic Publishers, Dordrecht-Boston-London, 380 pp, 2002.

Nickolaenko, A. P., Hayakawa, M., and Sekiguchi, M.: Variations in global thunderstorm activity inferred from the OTD records, Geophys. Res. Lett., 33, L06823, doi:10.1029/2005GL024884, 2006.

Pechony, O., Price, C., and Nickolaenko, A. P.: Model variations of Schumann resonance based on OTD maps of the global lightning activity, J. Geophys. Res., 111, D23102, doi:10.1029/2005JD006844, 2006.

Pechony, O. and Price, C.: Schumann resonances: interpretation of local intensity modulations, Radio Sci., 41, RS2S05, doi:10.129/2006RS003455, 2006 (printed 42(2), 2007).

Polk, C. and Fitchen, F.: Schumann resonances of the Earth-ionosphere cavity – Extremely low frequency reception at Kingston, R.I., J. Res. Nat. Bur. Stand. U.S., Sect. D, 66, 313–318, 1962.

Polk, C.: Relation of ELF noise and Schumann resonances to thunderstorm activity, Planetary Electrodynamics, edited by: Coronoti, S. and Hughes, J., vol.2, Ch.6, 55–83, Gordon and Breach, New York, 1969.

Sentman, D. D. and Fraser, B. J.: Simultaneous observation of Schumann resonances in California and Australia: evidence for intensity modulation by local height of D region, J. Geophys. Res,, 96(9), 15 973–15 984, 1991.

Yatsevich, E. I., Nickolaenko, A. P., Shvets, A. V., and Rabinowicz, L. M.: Two component source model of Schumann resonance signal, J. Atmos. Electr., 26(1), 1–10, 2006.